

1 **Triple oxygen isotope distribution in modern mammal teeth and potential geologic**
2 **applications**

3

4

5 **Authors**

6 Sophie B. Lehmann¹, Naomi E. Levin², Benjamin H. Passey², Huanting Hu³, Thure E. Cerling^{4, 5},
7 Joshua H. Miller⁶, Laura Arppe⁷, Emily J. Beverly⁸, Kathryn A. Hoppe^{9,10}, Julie Luyt¹¹, Judith Sealy¹¹

8

9

10 **Affiliations**

11 ¹Department of Geology and Environmental Science, University of Pittsburgh, Pittsburgh, PA,
12 15260; sophie.b.lehmann@gmail.com

13 ²Department of Earth and Environmental Sciences, University of Michigan, 1100 North
14 University Avenue, Ann Arbor, MI, 48103, USA; passey@umich.edu, nelevin@umich.edu

15 ³School of Oceanography, Shanghai Jiao Tong University; huanting.hu@sjtu.edu.cn

16 ⁴Department of Biology and ⁵Department of Geology and Geophysics, University of Utah, Salt
17 Lake City, UT 84112; thure.cerling@utah.edu

18 ⁶Department of Geology, University of Cincinnati, Cincinnati, Ohio, 45221, USA;
19 josh.miller@uc.edu

20 ⁷ Finnish Museum of Natural History, University of Helsinki, Helsinki, Finland;
21 laura.arppe@helsinki.fi

22 ⁸ Department of Earth and Atmospheric Sciences, University of Houston, Houston, Texas 77204;

23 ejbeverly@uh.edu

24 ⁹ Green River College and ¹⁰ Burke Museum, University of Washington; khoppe@greenriver.edu

25 ¹¹ Department of Archaeology, University of Cape Town, South Africa; Julie.luyt@uct.ac.za,

26 Judith.Sealy@uct.ac.za

27

28

29 **Highlights**

30 • We present $\Delta'{}^{17}\text{O}$ data from 50 teeth from 7 mammal families and 3 continents.

31 • $\Delta'{}^{17}\text{O}_{\text{enamel}}$ values of animals from a single environment span up to 146 per meg.

32 • $\Delta'{}^{17}\text{O}_{\text{enamel}}$ is insensitive to geographic variables affecting $\delta^{18}\text{O}_{\text{meteoric water}}$.

33 • $\Delta'{}^{17}\text{O}_{\text{enamel}}$ from arid sites are lower and more variable than from mesic sites.

34 • $\Delta'{}^{17}\text{O}_{\text{enamel}}$ can be used as an indicator of aridity.

35

36

37 **Keywords**

38 Aridity, mammalian teeth, paleoclimate, environment, stable isotopes, triple oxygen isotopes

39

40 **Abstract**

41 Reconstructing water availability in terrestrial ecosystems is key to understanding past
42 climate and landscapes, but there are few proxies for aridity that are available for use at
43 terrestrial sites across the Cenozoic. The isotopic composition of tooth enamel is widely used as
44 paleoenvironmental indicator and recent work suggests the potential for using the triple
45 oxygen isotopic composition of mammalian tooth enamel ($\Delta'^{17}\text{O}_{\text{enamel}}$) as an indicator of aridity.
46 However, the extent to which $\Delta'^{17}\text{O}_{\text{enamel}}$ values vary across environments is unknown and there
47 is no framework for evaluating past aridity using $\Delta'^{17}\text{O}_{\text{enamel}}$ data. Here we present $\Delta'^{17}\text{O}_{\text{enamel}}$ and
48 $\delta^{18}\text{O}_{\text{enamel}}$ values from 50 extant mammalian herbivores that vary in physiology, behavior, diet,
49 and water-use strategy. Teeth are from sites in Africa, Europe, and North America and
50 represent a range of environments (humid to arid) and latitudes (34°S to 69°N), where mean
51 annual $\delta^{18}\text{O}$ values of meteoric water range from -26.0‰ to 2.2‰ (VSMOW). $\Delta'^{17}\text{O}_{\text{enamel}}$ values
52 from these sites span 154 per meg (-291 to -137 per meg, where 1 per meg = 0.001‰). The
53 observed variation in $\Delta'^{17}\text{O}_{\text{enamel}}$ values increases with aridity, forming a wedged-shape pattern
54 in a plot of aridity index vs. $\Delta'^{17}\text{O}_{\text{enamel}}$ that persists regardless of region. In contrast, the plot of
55 aridity index vs. $\delta^{18}\text{O}_{\text{enamel}}$ for these same samples does not yield a distinct pattern. We use these
56 new $\Delta'^{17}\text{O}_{\text{enamel}}$ data from extant teeth to provide guidelines for using $\Delta'^{17}\text{O}_{\text{enamel}}$ data from fossil
57 teeth to assess and classify the aridity of past environments. $\Delta'^{17}\text{O}_{\text{enamel}}$ values from the fossil
58 record have the potential to be a widely used proxy for aridity without the limitations inherent
59 to approaches that use $\delta^{18}\text{O}_{\text{enamel}}$ values alone. In addition, the data presented here have
60 implications for how $\Delta'^{17}\text{O}_{\text{enamel}}$ values of large mammalian herbivores can be used in
61 evaluations of diagenesis and past $p\text{CO}_2$.

62 **1. Introduction and Background**

63 *1.1. Traditional use of oxygen isotopes in tooth enamel as climatic and environmental proxies*

64 The distribution of oxygen isotopes in marine and terrestrial carbonates (e.g.,
65 foraminifera tests, soil and lake carbonates, tooth enamel) has long been used to reconstruct
66 climate, environment, and surface processes (e.g., Zachos et al., 2001; Rowley and Currie, 2006;
67 Blumenthal et al., 2017). Oxygen isotope values ($\delta^{18}\text{O}$) of carbonate vary with environmental
68 conditions and geography because they reflect the $\delta^{18}\text{O}$ value of the waters from which they
69 form. The $\delta^{18}\text{O}$ value of meteoric-derived waters (e.g., rain, rivers, lakes, groundwater) varies
70 relative to climate and hydrology because it is sensitive to both equilibrium (e.g., temperature
71 changes, Rayleigh distillation) and kinetic (e.g., evaporation) oxygen isotope fractionation
72 effects (e.g., Rozanski et al., 1993). However, the influence of these isotope effects on the $\delta^{18}\text{O}$
73 values can be difficult to tease apart.

74 Fossil mammalian teeth are found globally, span the Cenozoic, and are used as
75 environmental indicators. The $\delta^{18}\text{O}$ value of tooth enamel ($\delta^{18}\text{O}_{\text{enamel}}$) is an alluring climate proxy
76 because it often tracks $\delta^{18}\text{O}$ values of meteoric water, but this relationship is sensitive to an
77 animal's diet, physiology, and water-use strategy (Kohn, 1996). An individual's $\delta^{18}\text{O}_{\text{enamel}}$ values
78 and their use as paleoclimate indicators are impacted by a variety of factors, including the
79 animal's intake of atmospheric O₂ (accounting for 5–40% of oxygen in body water), its water-
80 use efficiency, and the degree of evaporation of ingested waters (plant waters, surface waters)
81 relative to local precipitation. Because $\delta^{18}\text{O}_{\text{enamel}}$ values have a variety of influences, they have
82 been used to track a range of processes. Some studies estimate changes in paleotemperature
83 from $\delta^{18}\text{O}_{\text{enamel}}$ values, relying on the assumption that $\delta^{18}\text{O}_{\text{enamel}}$ values track the $\delta^{18}\text{O}$ value of

84 meteoric water, which vary with temperature at mid to high latitudes (e.g., Fricke et al., 1995).
85 However, this approach does not account for variability in $\delta^{18}\text{O}$ values of ingested waters within
86 an ecosystem, where leaf and drinking waters can be several per mil (‰) higher than
87 unevaporated meteoric water. Other approaches leverage these differences in evaporation and
88 use $\delta^{18}\text{O}_{\text{enamel}}$ values from animals with different diets and behaviors to separate the influence of
89 evaporative enrichment on $\delta^{18}\text{O}_{\text{enamel}}$ values and then estimate past aridity (Levin et al., 2006;
90 Blumenthal et al., 2017). This "aridity index" approach categorizes animals by their water-use
91 strategy where evaporation-insensitive (EI) taxa, like Hippopotamidae, ingest a relatively large
92 amount of drinking water, in contrast to evaporation-sensitive (ES) taxa, like Giraffidae, which
93 require less drinking water. The offset between $\delta^{18}\text{O}_{\text{enamel}}$ values of ES and EI taxa increases with
94 aridity. While the $\delta^{18}\text{O}_{\text{enamel}}$ aridity indicator is powerful, it is tuned to Quaternary mammal
95 assemblages in eastern Africa (Blumenthal et al., 2017) and not easily transferrable to older
96 periods or different regions without making assumptions about animal behavior and
97 physiology.

98

99 1.2. Triple oxygen isotopic composition of waters and carbonates

100 Triple oxygen isotope ($^{18}\text{O}-^{17}\text{O}-^{16}\text{O}$) distributions in water and near-surface minerals (e.g.,
101 carbonate, gypsum) have potential as indicators of aridity because they are sensitive to kinetic
102 and equilibrium isotope effects and can track the influence of evaporation (Barkan and Luz,
103 2005; 2007; Li et al., 2017; Surma et al., 2018; Passey and Levin, 2021).

104 The majority of processes involving oxygen isotopic fractionation on Earth are mass
105 dependent and governed by the power law relationship $^{17}\alpha_{a-b} = {^{18}\alpha_{a-b}}^{\theta}$, where the isotopic

106 fractionation between two materials or phases, a and b, is defined as $\alpha_{a-b} = R_a/R_b$ and R
107 represents the ratio of the heavy to light isotope ($^{18}\text{O}/^{16}\text{O}$, $^{17}\text{O}/^{16}\text{O}$) (Matsuhisa et al., 1978;
108 Young et al., 2002). Although these relationships have been well known for the past 40 years,
109 differences in the exponent θ were considered too small to detect with most analytical
110 approaches and there was little motivation for analyzing $\delta^{17}\text{O}$ as it provided the same
111 information as $\delta^{18}\text{O}$. However, efforts to increase analytical precision yield empirical and
112 experimental studies that showed measurable distinctions in θ between kinetic and equilibrium
113 fractionation processes. These distinctions are particularly evident in the hydrosphere where θ
114 is 0.529 for equilibrium exchange between water liquid and vapor, but 0.5185 for the diffusion
115 of water through air that occurs during evaporation (Young et al., 2002; Barkan and Luz, 2005;
116 2007).

117 These θ values are equivalent to the slope on a $\delta'^{18}\text{O}$ - $\delta'^{17}\text{O}$ plot, where $\delta^x\text{O} = (R_{\text{sample}}/$
118 $R_{\text{standard}} - 1) * 1000$ and $\delta'^x\text{O} = \ln(R_{\text{sample}}/R_{\text{standard}})$, and $x = 17$ or 18 . Given the small distinctions in
119 slope that differentiate equilibrium and kinetic fractionation (0.529 vs. 0.5185), we use $\Delta'^{17}\text{O}$ to
120 visualize and discuss triple oxygen isotope variation, where λ represents the slope in the $\delta'^{18}\text{O}$ -
121 $\delta'^{17}\text{O}$ plot and is the mathematical equivalent to θ (Miller, 2002). Larger deviations and more
122 negative $\Delta'^{17}\text{O}$ values reflect a greater influence of evaporation (Figs. 1-2). In this study, we use
123 λ instead of θ to characterize $^{18}\text{O}-^{17}\text{O}-^{16}\text{O}$ distributions because it represents the relationship
124 between the fractionation of $^{18}\text{O}/^{16}\text{O}$ and $^{17}\text{O}/^{16}\text{O}$ values during a combination of processes,
125 whereas θ characterizes this relationship for a single process (Barkan and Luz, 2005; 2007).

126 Meteoric-derived waters like rain, river, lake and ground waters have $\Delta'^{17}\text{O}$ values that
127 range from -56 to +60 per meg (Landais et al., 2006, 2010; Barkan and Luz, 2011; Surma et al.,

128 2015, 2018; Li et al., 2017; Passey and Ji, 2019; Uechi and Uemura, 2019). However, exceptions
129 include evaporated ponds in the Atacama Desert and in the Sistan Oasis that yield much lower
130 $\Delta'^{17}\text{O}$ values (~-70 per meg and -167 per meg, respectively) (Surma et al., 2015; 2018; Herwartz
131 et al., 2017). Plant water $\Delta'^{17}\text{O}$ values are typically more sensitive to evaporation than meteoric-
132 derived waters, ranging from -271 to +35 per meg (Fig. 1).

133 Similar to $\delta^{18}\text{O}_{\text{enamel}}$ values, $\Delta'^{17}\text{O}$ values of mammalian tooth enamel ($\Delta^{17}\text{O}_{\text{enamel}}$) are
134 influenced by the isotopic composition of food, drinking water, and atmospheric O_2 (Pack et al.,
135 2013). The $\Delta'^{17}\text{O}$ value of O_2 is distinct and considerably lower than water, with a value of
136 -432±15 per meg (1 σ) recommended by Pack (2021) based on a compilation of data from the
137 recent literature (Fig. 1). Relative humidity has a particularly strong influence on body water
138 $\Delta'^{17}\text{O}$ values of mammalian herbivores because it reflects the degree of evaporation of ingested
139 water (Passey and Levin, 2021; Hu et al., *in revision*).

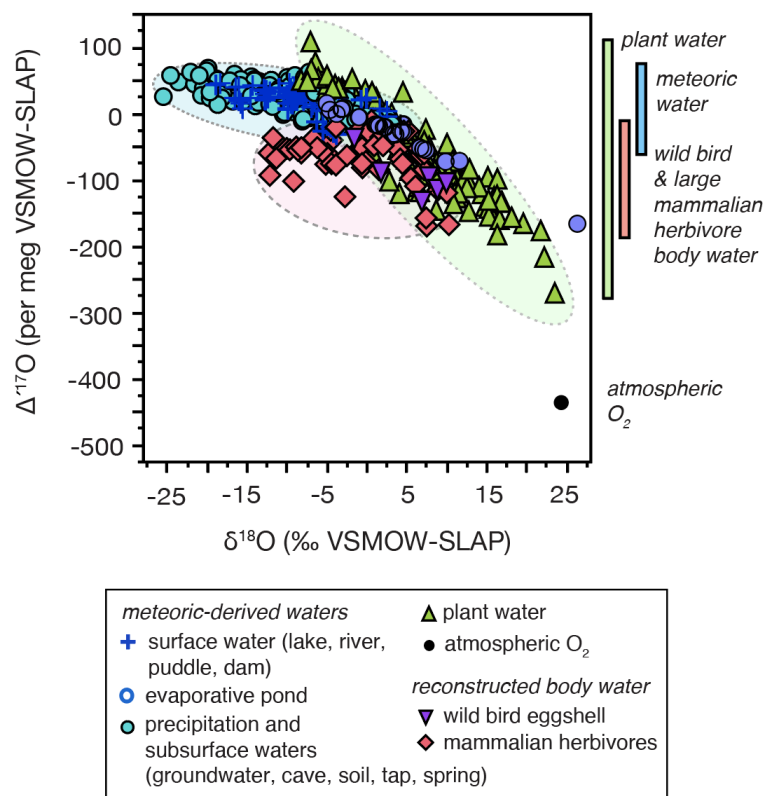
140 Given the strong influence of evaporation on the oxygen isotopes of body water, we
141 expect $\Delta'^{17}\text{O}_{\text{enamel}}$ values to vary with environment (Fig. 2B) such that they can be used as
142 indicators of past aridity. Models of isotopic fractionation in body water suggest that animals
143 who ingest the majority of their water from plants should have more negative $\Delta'^{17}\text{O}_{\text{enamel}}$ values
144 than animals that drink water regularly due to evaporative enrichment of plant/leaf water
145 relative to surface waters (Passey and Levin, 2021; Hu et al., *in revision*; Fig. 2C). Given this, we
146 predict that $\Delta'^{17}\text{O}_{\text{enamel}}$ values will exhibit more variance in arid environments regardless of taxa
147 and meteorological/climatic features that vary according to geographic location of a site.

148 Here we present the $\Delta'^{17}\text{O}_{\text{enamel}}$ values of teeth from 50 extant herbivores from seven
149 mammalian families and three continents to demonstrate variation in $\Delta'^{17}\text{O}_{\text{enamel}}$ values across

150 different environments. We then outline approaches to using $\Delta'{}^{17}\text{O}_{\text{enamel}}$ records to reconstruct
151 past aridity, in addition to its use in assessing post-depositional alteration of enamel oxygen
152 isotopes and as a $p\text{CO}_2$ indicator.

153

154

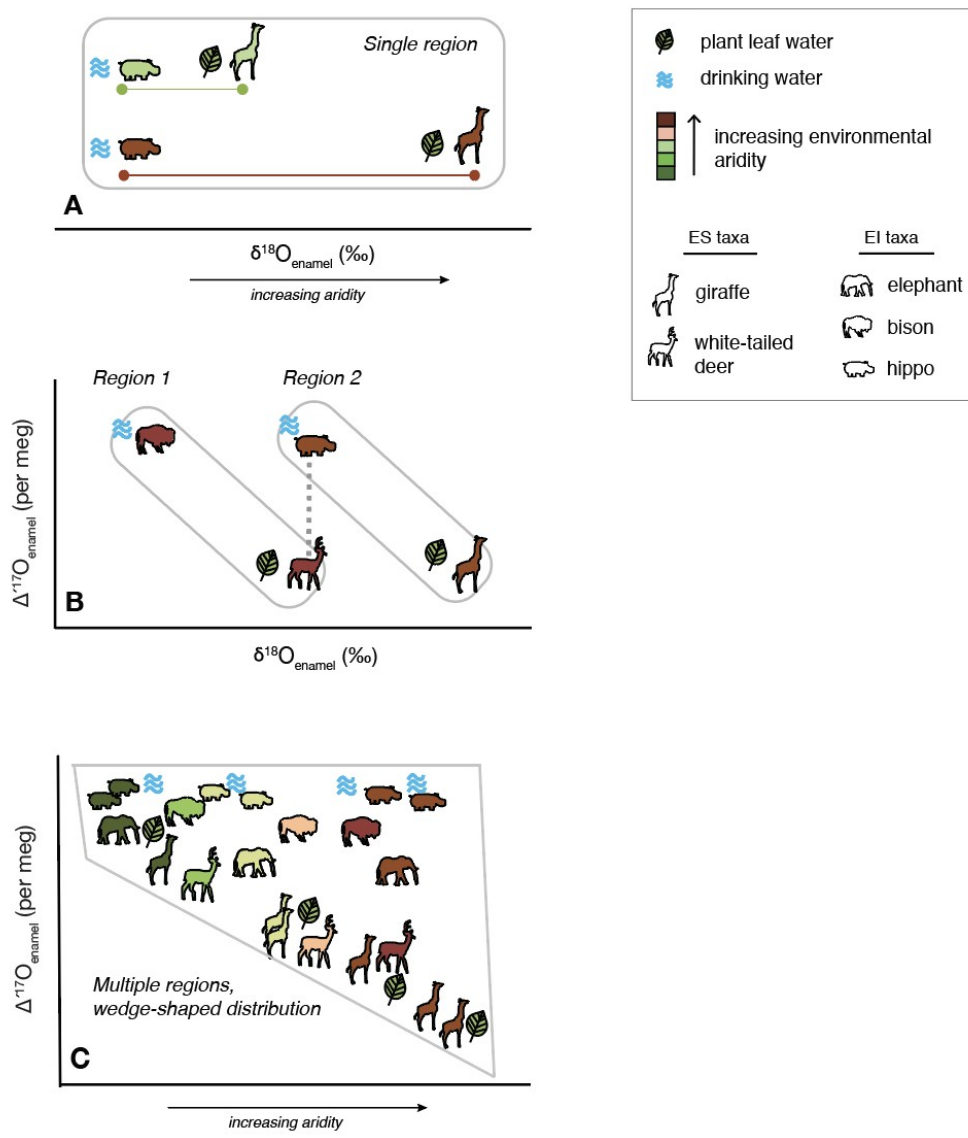


155

156

157 **Figure 1:** $\Delta'{}^{17}\text{O}$ and $\delta^{18}\text{O}$ values of reconstructed body water for extant mammalian herbivores
158 and birds and their primary input sources of oxygen: ingested plant water and drinking water,
159 and inhaled atmospheric O_2 . Body water $\Delta^{17}\text{O}$ values are calculated from teeth and eggshells
160 ($BW \Delta'{}^{17}\text{O} = \Delta'{}^{17}\text{O}_{\text{enamel or eggshell}} - (\lambda - 0.528) * (1000 * \ln(^{18}\alpha))$, where $\lambda = 0.5245$, $^{18}\alpha = 1.0332$ for
161 teeth, and $^{18}\alpha = 1.0332$ for eggshells as in Passey et al. (2014)). Meteoric-derived waters are

162 separated into the categories precipitation and subsurface waters, surface waters, and
 163 evaporative ponds. Vertical bars on right show the range of $\Delta^{17}\text{O}$ values for sources of oxygen
 164 for mammals and their reconstructed body waters. Data are from Landais et al. (2006, 2010),
 165 Luz and Barkan (2010), Barkan and Luz (2011), Passey et al. (2014), Li et al. (2017), Surma et al.
 166 (2015; 2018), Herwartz et al. (2017), Passey and Ji (2019), Uechi and Uemura (2019), Whiteman
 167 et al. (2019), Pack et al. (2021); Hu et al. (*in revision*), and this study.



168

169

170 **Figure 2:** Schematics outlining the variation of $\delta^{18}\text{O}_{\text{enamel}}$ and $\Delta'^{17}\text{O}_{\text{enamel}}$ values with aridity. A)
171 The $\delta^{18}\text{O}_{\text{enamel}}$ value of evaporative sensitive (ES) and evaporative insensitive (EI) taxa from two
172 environments within a single region where the $\delta^{18}\text{O}$ value of drinking water is constant. B) The
173 $\delta^{18}\text{O}_{\text{enamel}}$ and $\Delta'^{17}\text{O}_{\text{enamel}}$ values of ES and EI taxa from environments with the same degree of
174 aridity but from different regions, where $\delta^{18}\text{O}$ values of drinking water vary. Dashed gray line
175 indicates how $\delta^{18}\text{O}_{\text{enamel}}$ values cannot distinguish a circumstance where aridity and input $\delta^{18}\text{O}$
176 values vary, whereas this distinction can be made with $\Delta'^{17}\text{O}_{\text{enamel}}$ values. C) Variation in
177 $\Delta'^{17}\text{O}_{\text{enamel}}$ values vs. aridity for various locations and taxa spanning a range of behaviors and
178 water-use strategies, showing a predicted wedge-shaped pattern.

179

180

181 **2. Materials and Methods**

182 *2.1. Site and sample selection*

183 We designed our sample selection to evaluate the triple oxygen isotope distribution of teeth
184 from large (> 6 kg), extant mammalian herbivores that represented a range of water-use
185 strategies and behaviors, continents, latitudes, and climates (Supplementary Table 1). We
186 analyzed teeth from Hippopotamidae ($n=4$), Elephantidae ($n=9$), Bovidae ($n=9$), Castoridae
187 ($n=2$), Cervidae ($n=15$) and Giraffidae ($n=6$). These data were combined with already published
188 data from a Hippopotamidae, Bovidae, and Rhinocerotidae from Passey et al. (2014) and a
189 Cervidae and Bovidae from Hu et al. (*in revision*). Teeth were collected over the past five
190 decades and many samples have been used in previous studies (Supplementary Table 2).
191 Specimens from Europe are from the Finnish Museum of National History.

192

193 2.2. Climate and aridity of sites

194 The geographic and climatic parameters for sites for which we report tooth enamel
195 triple oxygen isotope data are listed in Table 1. We extracted mean annual temperature (MAT),
196 precipitation (MAP), potential evapotranspiration (PET), percent relative humidity (rh), and
197 Aridity Index (AI, where AI=MAP/PET) estimates for each location using the WorldClim Global
198 Climate Data raster 1.4, or WorldClim1.4 (Hijmans et al., 2005; Trabucco and Zomer, 2009). We
199 assigned corresponding UNESCO climate classifications to sites using AI data: arid, semi-arid,
200 subhumid, and humid (UNESCO, 1979). The $\delta^{18}\text{O}$ values of mean annual meteoric water (‰
201 VSMOW) were calculated using waterisotopes.org (Bowen and Revenaugh, 2003).

202

203 2.3. Sample preparation and analysis

204 Enamel was removed along the growth axis of the tooth, cleared of dentine and dirt,
205 powdered, and homogenized. Powder was treated with 3% H_2O_2 to remove organic material,
206 bathed in buffered acetic acid (0.1 M) to remove secondary carbonate, and dried at 60°C. Analysis
207 of triple oxygen isotopes of enamel followed the procedure outlined in Passey et al. (2014). Briefly,
208 enamel powder (140 – 200 mg per analysis) was placed in silver capsules and reacted in a common
209 bath of 100% phosphoric acid under vacuum at 90°C to extract CO_2 . CO_2 was then reduced to H_2O
210 (Fe powder catalyst, 560°C, 20 minutes), which was then fluorinated by passing through cobalt
211 trifluoride at 370°C. The resultant O_2 was then analyzed by dual inlet isotope ratio mass
212 spectroscopy on a Thermo Scientific MAT 253 at Johns Hopkins University. Samples were analyzed
213 in duplicate. We evaluated the stability of isotope measurements of external carbonate standards,

214 both international (NBS18 and NBS19) and in-house (102-GC-AZ01) carbonates, and an inhouse
215 CO₂ gas standard (Tank#2 CO₂). Water standards SLAP2 and VSMOW2 were directly injected into
216 the cobalt trifluoride reactor to produce O₂ gas. The pooled standard deviation (1 σ) for the
217 external carbonate and CO₂ standards was 0.9‰ for $\delta^{18}\text{O}$ and 10 per meg for $\Delta^{17}\text{O}$ over the time
218 period when the samples were analyzed.

219 Carbonate oxygen isotope data were normalized to VSMOW2 ($\delta^{18}\text{O}=0\text{\textperthousand}$ and $\delta^{17}\text{O}=0$ per
220 meg) and scaled to SLAP2 ($\delta^{18}\text{O}=-55.5\text{\textperthousand}$) using the reference frame $\Delta^{17}\text{O}_{\text{SLAP2}}=0$ per meg, where
221 $\delta^{17}\text{O}_{\text{SLAP2}}=-29.6986\text{\textperthousand}$ when $\delta^{18}\text{O}_{\text{SLAP2}}=-55.5\text{\textperthousand}$ and $\lambda=0.528$ (Schoenemann et al., 2013). A secondary
222 normalization step was performed for carbonates to correct for offsets between observed and
223 accepted $\delta^{18}\text{O}$ values (Passey et al., 2014). Finally, we compared $\Delta^{17}\text{O}$ of international and internal
224 standards analyzed during each session to values reported in Passey et al., 2014 (NBS18=-98 per
225 meg; NBS19=-135 per meg; 102-GC-AZ01=-94 per meg; Tank#2 CO₂=118 per meg). If a significant
226 difference was observed, we applied a correction to all carbonate $\Delta^{17}\text{O}$ data from that session
227 based on the residual from the Passey et al. (2014) $\Delta^{17}\text{O}$ values, averaged for all standards
228 analyzed within that session. Of the six analytical sessions in this study, three required such
229 correction, with magnitudes of -40 per meg (July 2015), -13 per meg (August 2015 session 1), and -
230 31 per meg (August 2015 session 2). We note that Wostbrock et al. (2020) report $\Delta^{17}\text{O}$ values for
231 CO₂ extracted from NBS18 and NBS19 (25°C reaction) with phosphoric acid of -100 per meg and -
232 155 per meg, respectively (compared to -98 per meg and -135 per meg in Passey et al., 2014).
233 Sharp and Wostbrock (2021) recommend normalizing $\Delta^{17}\text{O}$ data to the values reported in
234 Wostbrock et al. (2020). We fundamentally agree with this recommendation, but refrain here
235 because our samples were reacted using a different phosphoric acid temperature (90°C instead of

236 25°C in Wostbrock and Sharp, 2020), and it is yet unknown how triple oxygen isotope acid
237 fractionation scales with temperature of acid digestion. Regardless, all data for standards are
238 reported Supplementary Table 3, which will allow for subsequent renormalization of our dataset
239 when the necessary fractionation factors are determined.

240 All data from analytical sessions are reported in Supplementary Table 4 (i.e., raw and
241 corrections). Data were evaluated using the statistical analytical software JMP 11 produced by
242 the SAS Institute. The \pm symbol indicates one standard deviation from the mean and data are
243 frequently reported as mean $\pm 1\sigma$. Throughout the text, oxygen isotope measurements are
244 described using $\Delta'^{17}\text{O}$ and $\delta^{18}\text{O}$ notation, δ -values are reported in per mil (\textperthousand), and $\Delta'^{17}\text{O}$ values
245 are reported in per meg, where 1 \textperthousand is 1000 per meg and defined with a reference slope of
246 0.528.

247 We used pairwise analyses to evaluate isotopic differences between latitudes, families, and
248 climate categories. However, while our $\delta^{18}\text{O}_{\text{enamel}}$ data are normally distributed, our $\Delta'^{17}\text{O}_{\text{enamel}}$ data
249 deviate from normality (Supplementary Fig. 1). Due to these differences, we use parametric
250 ANOVA tests to evaluate $\delta^{18}\text{O}_{\text{enamel}}$ and nonparametric Wilcoxon and Kruskal-Wallis tests to
251 evaluate $\Delta'^{17}\text{O}_{\text{enamel}}$. Differences among-group were evaluated using Tukey-Kramer HSD and the
252 Steel-Dwass Method. To test for differences in variance across climate, we used the parametric
253 Bartlett's test and nonparametric Levene's test for $\delta^{18}\text{O}_{\text{enamel}}$ and $\Delta'^{17}\text{O}_{\text{enamel}}$, respectively. Within
254 each family, we used linear regression to evaluate the relationship between changes in aridity and
255 associated changes in isotope values. All isotope values from a common family at a single site are
256 first summarized as the median value before evaluating the linear regression to account for non-
257 independence.

258

259

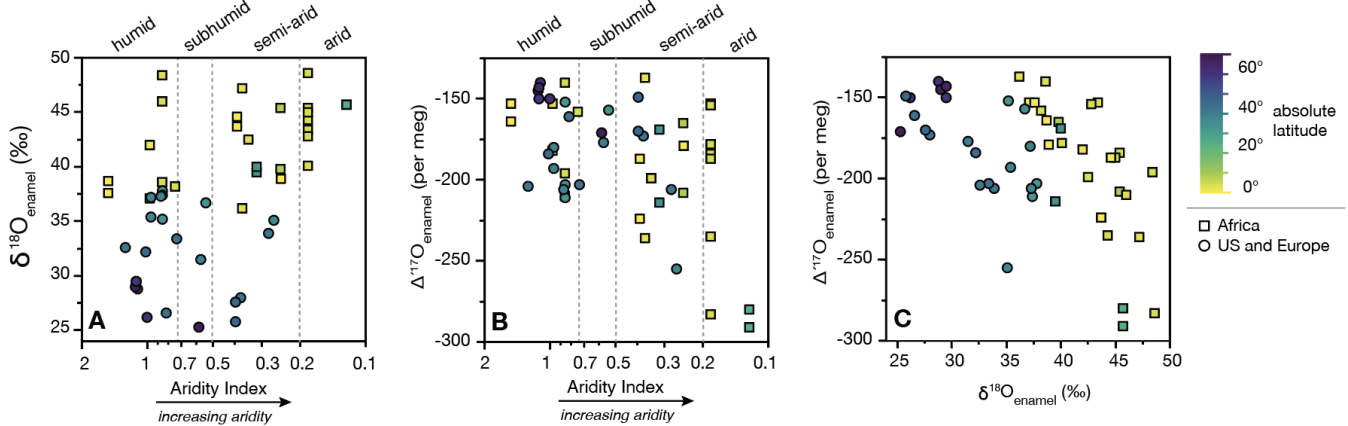
260 **3. Results**

261 *3.1. Variation by latitude and region*

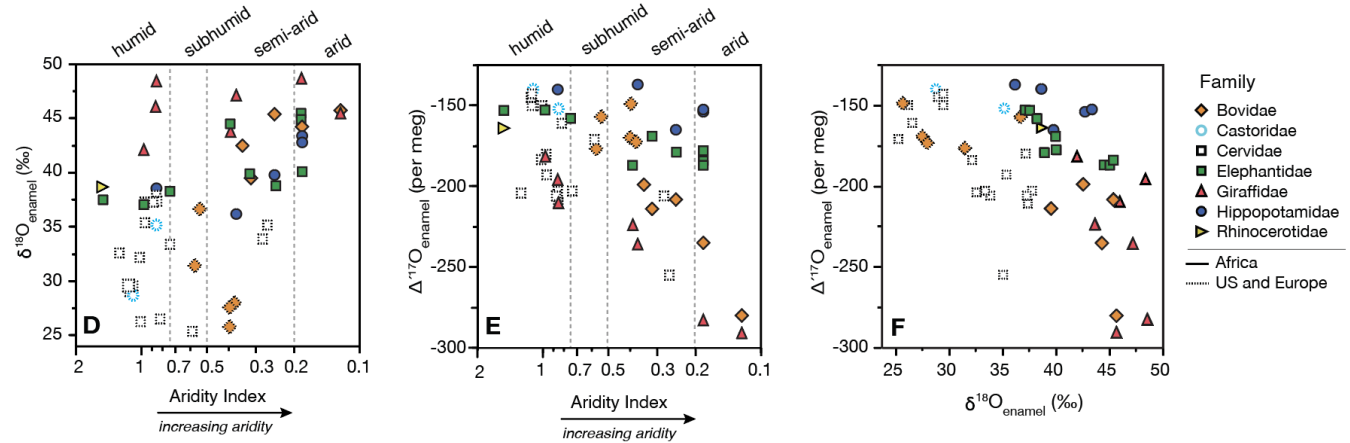
262 Among all the herbivores, $\Delta^{17}\text{O}_{\text{enamel}}$ values range from -291 to -137 per meg (-186 ± 37
263 per meg) and $\delta^{18}\text{O}_{\text{enamel}}$ values range from 25.3‰ to 48.6‰ (37.6 ± 6.6 ‰) (Supplementary Table
264 1; Fig. 3). $\Delta^{17}\text{O}_{\text{enamel}}$ values do not vary with absolute latitude ($R^2=0.017$, $p=0.1965$). $\delta^{18}\text{O}_{\text{enamel}}$
265 values decrease with increasing absolute latitude ($R^2=0.628$, $p=<0.0001$), such that teeth
266 sampled from low latitudes ($0 - 24^\circ$, $n=24$) yield $\delta^{18}\text{O}_{\text{enamel}}$ values that are significantly different
267 ($p>0.0001$) than those from mid latitudes ($24 - 66^\circ$, $n=21$) (Fig. 3 A – C). The lack of obvious
268 differences in the $\delta^{18}\text{O}_{\text{enamel}}$ values from mid and high latitudes may be an artifact of limited
269 samples from high latitudes ($> 66^\circ$, $n=3$).

270

By absolute latitude, continent, and climate



By taxon, continent, and climate



271

272

273 **Figure 3:** Distribution of $\delta^{18}\text{O}_{\text{enamel}}$ and $\Delta^{17}\text{O}_{\text{enamel}}$ values by latitude, location, taxon, and climate.

274 In plots A – C, the geography of sample site is indicated using a color gradient for absolute
 275 latitude and symbols according to region. In plots D – F, taxa are grouped by family. Aridity
 276 Index is presented on a log scale and corresponding UNESCO climate categories are separated
 277 by vertical dashed lines.

278

279

280 3.2. Variation by aridity

281 Teeth come from a range of environments where AI values range from 0.12 to 1.52
282 (Table 1). Environments were placed into UNESCO climate classifications using AI data and
283 characterized as humid ($AI > 0.75$, $n=22$), subhumid ($AI 0.5 - 0.75$, $n=3$), semi-arid ($AI 0.2 - 0.5$,
284 $n=16$), and arid ($AI < 0.2$, $n=9$) (UNESCO, 1979). They include the arid Turkana and Kgalagadi
285 regions ($AI 0.18$ and 0.12 , respectively), mid latitude semi-arid Utah ($AI 0.26$), high latitude,
286 cold, subhumid Alaska ($AI 0.58$), moist highlands in Kenya ($AI 1.51$), and cool, humid Finland (AI
287 > 1.01).

288 The distribution of $\Delta'{}^{17}\text{O}_{\text{enamel}}$ values form a wedge-shaped pattern when plotted against
289 AI. $\Delta'{}^{17}\text{O}_{\text{enamel}}$ values from arid and semi-arid sites ($n=25$, -283 to -137 per meg, -196 ± 43 per
290 meg) have statistically different variance from subhumid and humid sites ($n=25$, -210 to -138
291 per meg, -170 ± 24 per meg) ($df=1$, $F=7.4179$, $p=0.0090$). The $\delta^{18}\text{O}_{\text{enamel}}$ values from more arid
292 sites (25.5 to $47.5\text{\textperthousand}$, $39.5 \pm 6.0\text{\textperthousand}$) are not different from more mesic sites (25.0 to $47.2\text{\textperthousand}$,
293 $34.2 \pm 5.7\text{\textperthousand}$) ($df=1$, $F=0.0063$, $p=0.9371$).

294

295 3.3. Variation by taxon

296 We observe that herbivore $\Delta'{}^{17}\text{O}_{\text{enamel}}$ and $\delta^{18}\text{O}_{\text{enamel}}$ values vary by taxonomy (Table 2;
297 Supplementary Table 5; Fig. 3 D – F).

298 In Africa, our sample includes giraffids ($n=7$), bovids ($n=5$), a rhinocerotid ($n=1$),
299 elephantids ($n=9$) and hippopotamids ($n=5$) from South Africa, Kenya, Uganda, and the
300 Democratic Republic of the Congo. The $\Delta'{}^{17}\text{O}_{\text{enamel}}$ values of hippopotamids are similar to
301 elephantids ($p=0.3766$) and are significantly higher than those of giraffids ($p=0.0295$). Giraffid
302 and bovid $\Delta'{}^{17}\text{O}_{\text{enamel}}$ values are similar ($p=0.9620$) and show large ranges in $\Delta'{}^{17}\text{O}_{\text{enamel}}$ (> 100 per

303 meg). In these groupings, giraffids include samples of giraffe and okapi while the bovids include
304 samples from buffalo, wildebeest, oryx and hartebeest. Giraffid and bovid $\Delta^{17}\text{O}_{\text{enamel}}$ values are
305 negatively correlated with AI (bovids, $R^2=0.950$, $p=0.0031$; giraffids, $R^2=0.860$, $p=0.0049$). In
306 contrast, $\Delta^{17}\text{O}_{\text{enamel}}$ values for elephantids and hippopotamids exhibit a narrow range across AI
307 (< 35 per meg) and have $R^2=0.467$ ($p=0.0543$) and $R^2=0.049$ ($p=0.3950$), respectively. The
308 distribution of $\delta^{18}\text{O}_{\text{enamel}}$ values of the different taxa mostly overlap with one another. The
309 correlations between $\delta^{18}\text{O}_{\text{enamel}}$ values and AI are $R^2=-1.403$ ($p=0.5104$) for hippopotamids,
310 $R^2=0.316$ ($p=0.1097$) for elephantids, $R^2=0.360$ ($p=0.1691$) for bovids, and $R^2=0.0461$ ($p=0.3276$)
311 for giraffids.

312 The samples from North America and Europe include teeth from bovids ($n=5$), castorids
313 ($n=2$) and cervids ($n=16$). The $\Delta^{17}\text{O}_{\text{enamel}}$ values of castorids and bovids represent a tighter range
314 (-177 to -140 per meg, -160 ± 14 per meg) than that of cervids (-255 to -143 per meg, -185 ± 31
315 per meg). In comparison, the ranges of cervid and bovid $\delta^{18}\text{O}_{\text{enamel}}$ are similar across AI (dif
316 mean=2.414550, $p=0.507$). Castorids from humid environments and their $\delta^{18}\text{O}_{\text{enamel}}$ values
317 overlap with those of cervids and bovids from humid to semi-arid environments.

318 Although not visible on Figure 3, where data are grouped by family, it is important to
319 note that three species of cervids were sampled (moose $n=3$, reindeer/caribou $n=3$, and white-
320 tailed deer $n=10$) spanning humid to semi-arid environments. White-tailed deer yield lower
321 $\Delta^{17}\text{O}_{\text{enamel}}$ values than that of moose and reindeer/caribou. There is no equivalent distinction in
322 $\delta^{18}\text{O}_{\text{enamel}}$ values.

323

324

325 **4. Discussion**

326 **4.1. Variation of $\Delta'^{17}\text{O}_{\text{enamel}}$ values**

327 **4.1.1. Observations**

328 The $\Delta'^{17}\text{O}_{\text{enamel}}$ values from extant herbivores from Africa, Europe and North America
329 span 146 per meg (-283 to -137 per meg) and can vary by 146 per meg at sites with data from
330 multiple taxa. In comparison, the $\Delta'^{17}\text{O}$ values of plant waters span up to 189 per meg in a single
331 environment (Li et al., 2017) and are sensitive to variation in rh between environments
332 (Alexandre et al., 2018), while the $\Delta'^{17}\text{O}$ values of meteoric waters across all environments span
333 85 per meg (Landais et al., 2006; 2010; Luz and Barkan, 2010; Passey et al., 2014; Li et al. 2017;
334 Passey and Ji, 2019).

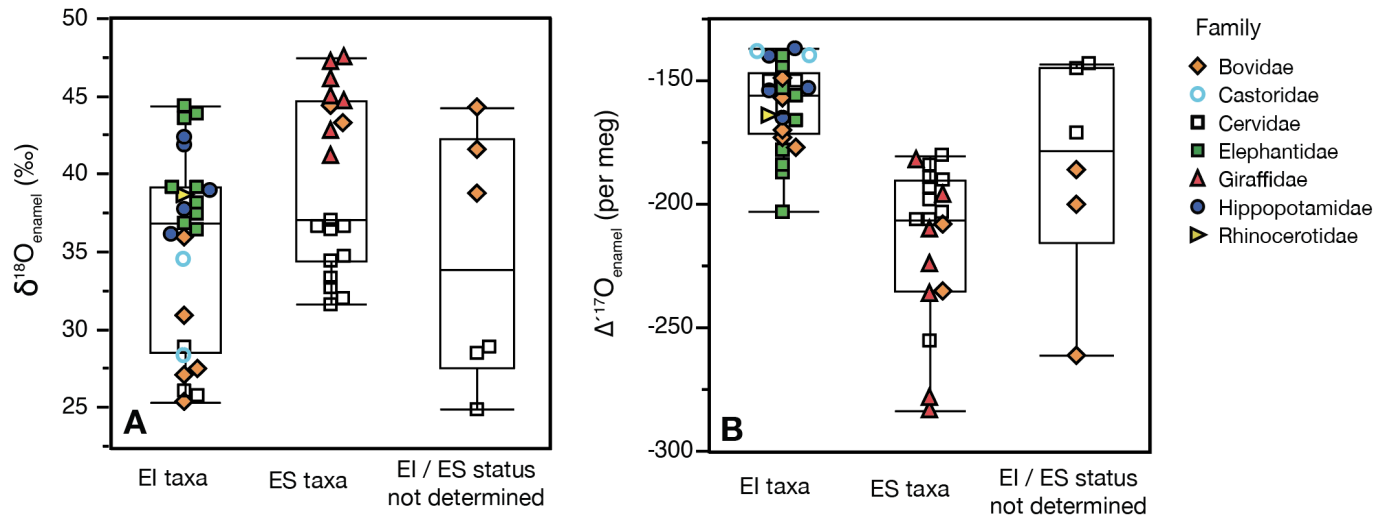
335 Aridity seems to be the strongest determinant of $\Delta'^{17}\text{O}_{\text{enamel}}$ values. We observe a greater
336 variation in $\Delta'^{17}\text{O}$ in arid and semi-arid environments, than in humid environments, resulting in
337 a wedge-shaped pattern in a plot of AI vs. $\Delta'^{17}\text{O}_{\text{enamel}}$ that persists across a range of latitudes and
338 $\delta^{18}\text{O}$ values of meteoric water (Fig. 3B). No similar relationship between $\delta^{18}\text{O}_{\text{enamel}}$ and aridity
339 exists (Fig. 3A). Instead, $\delta^{18}\text{O}_{\text{enamel}}$ more closely tracks latitude, reflecting the well-known
340 correlation between $\delta^{18}\text{O}$ values of meteoric water and latitude (e.g., Dansgaard, 1964).

341 This wedge-shaped $\Delta'^{17}\text{O}_{\text{enamel}}$ – aridity relationship occurs when taxa with a range of
342 water-use strategies are sampled. As discussed above, water-use strategy is influenced by diet,
343 physiology, and behavior. An important factor is a taxon's water dependence, which can be
344 characterized by the Water Economy Index (WEI), where WEI=ml H₂O ingested per kJ of
345 metabolic energy (see Nagy and Peterson, 1988). Animals with low WEI values are less
346 dependent on surface waters and can more readily sustain water requirements based on

347 dietary water (leaf water, root/stem water, metabolic water; Kohn, 1996). Oxygen isotope
348 distributions in animals generally group into two categories, evaporation sensitive (ES) and
349 evaporation insensitive (EI), where $\delta^{18}\text{O}_{\text{enamel}}$ values of EI taxa (high WEI) do not vary with aridity
350 and $\delta^{18}\text{O}_{\text{enamel}}$ values of ES taxa (low WEI) increase with aridity (Levin et al., 2006; Blumenthal et
351 al., 2017). We classify taxa as ES or EI using previously published work when possible and
352 otherwise assign a suggested ES or EI classification based on an animal's water and food intake
353 (Table 2).

354 When $\Delta'^{17}\text{O}_{\text{enamel}}$ data from the entire dataset are pooled and taxa are grouped by ES and
355 EI classification, $\Delta'^{17}\text{O}_{\text{enamel}}$ values of ES taxa are both lower and more varied than those of EI taxa
356 (Fig. 4A). The distinctions in $\Delta'^{17}\text{O}_{\text{enamel}}$ values between ES and EI taxa persist across the three
357 continents and the different climate regimes. In contrast, $\delta^{18}\text{O}_{\text{enamel}}$ values of ES and EI taxa are
358 not distinct, in part because they are strongly influenced by local meteoric water $\delta^{18}\text{O}$ values
359 which exert a stronger influence on $\delta^{18}\text{O}_{\text{enamel}}$ values than animal water-use strategies (Fig. 4B).
360 The clear distinctions in $\Delta'^{17}\text{O}_{\text{enamel}}$ values between ES and EI taxa show the importance of
361 including samples from taxa with a range of water-use strategies to assess the distribution of
362 $\Delta'^{17}\text{O}_{\text{enamel}}$ values from any location.

363



364

365

366 **Figure 4:** Box plots of A) $\delta^{18}\text{O}_{\text{enamel}}$ and B) $\Delta'^{17}\text{O}_{\text{enamel}}$ values of taxa grouped by the EI and ES
367 classification and plotted by family. Box ends are the quartile values, inner horizontal line the
368 median, and whiskers the range.

369

370

371 4.1.2. $\Delta'^{17}\text{O}_{\text{enamel}}$ values in light of the $\Delta'^{17}\text{O}$ body water model

372 Accurate isotope mass-balance body water models are critical for understanding the
373 controls on oxygen isotopic variation in tooth enamel. Of the body water models developed for
374 $\delta^{18}\text{O}$, some are scaled to body mass and metabolic rate (e.g., Bryant and Froelich, 1995),
375 whereas others consider animal behavior and physiology which can influence $\delta^{18}\text{O}$
376 independently of animal mass (e.g., Kohn, 1996). The latter is effective at predicting $\delta^{18}\text{O}_{\text{enamel}}$
377 across aridity gradients (e.g., Blumenthal et al., 2017) because it accounts for variation in fluxes
378 of water that undergo evaporation, including both water that is consumed (e.g., leaf waters,
379 surface waters) and released by an animal (e.g., vapor loss during breathing, panting).

380 With increased interest in triple oxygen isotopes, isotope mass-balance body water
381 models have been adapted to consider $\Delta^{17}\text{O}$, using approaches that either scale to animal mass
382 (Pack et al., 2013; Whiteman et al., 2019) or link to animal physiology and behavior (Passey and
383 Levin, 2021; Hu et al., *in revision*). While some studies demonstrate positive trends between
384 $\Delta^{17}\text{O}$ values of body water ($\Delta^{17}\text{O}_{\text{bw}}$) and body mass (Pack et al., 2013; Whiteman et al., 2019),
385 there is considerable scatter in $\Delta^{17}\text{O}_{\text{bw}}$ values (> 200 per meg) among animals that do not vary
386 in body mass but that do vary in WEI (Passey and Levin, 2021). This latter observation indicates
387 the importance of physiology, behavior, and environment in determining $\Delta^{17}\text{O}$ values in
388 animals, as has been observed for $\delta^{18}\text{O}$ (e.g., Luz et al., 1990; Levin et al., 2006; Blumenthal et
389 al., 2017).

390 Here we compare the $\Delta^{17}\text{O}_{\text{enamel}}$ results from this study to outputs from an isotope mass-
391 balance model to understand why $\Delta^{17}\text{O}_{\text{enamel}}$ values vary among different taxa and across
392 environmental gradients. We use a modeling approach that allows for the adjustment of fluxes
393 of oxygen in and out of animals based on a version of the Kohn (1996) model that is modified
394 for triple oxygen isotopes (Passey and Levin, 2021; Hu et al., *in revision*). We modeled animal
395 physiology and behavior in four different scenarios: 1) a standard evaporation-sensitive
396 condition where an animal is efficient with its water use (low WEI), has dry feces and consumes
397 a large relative fraction of leaf water (e.g., giraffe, deer); 2) a water-dependent animal with high
398 WEI, wet feces, but with a low proportion of consumed leaf water (e.g., hippos, beaver); 3)
399 another water-dependent condition where an animal has a high WEI and wet feces, but
400 consumes a high proportion of leaf water (e.g., elephant); and 4) an evaporation-sensitive
401 condition where an animal has low WEI and dry feces but consumes very little leaf water (e.g.,

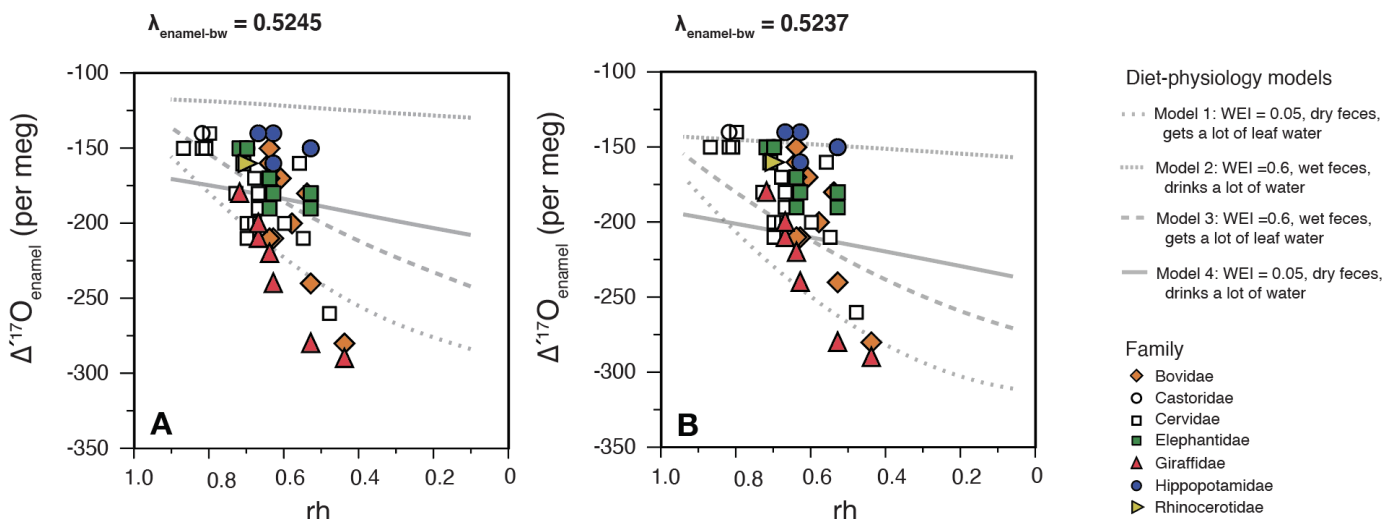
402 reindeer, caribou). These four different diet-physiology models are represented by the four
403 different lines in Figure 5A-B. Model conditions are presented in Supplementary Tables 6 and 7.
404 In these models, we use rh to represent environmental variation as it is a physical parameter
405 that controls oxygen isotope fractionation, in contrast to using the AI or water deficit terms
406 which are used to characterize environment of a particular place during average conditions
407 (Supplementary Table 8).

408 For comparison to our $\Delta'^{17}\text{O}_{\text{enamel}}$ results, we calculated the equivalent mineral (enamel)
409 composition from body water models using the $^{18/16}\alpha_{\text{enamel-bw}} = 1.0332$ and $\lambda_{\text{enamel-bw}} = 0.5245$,
410 using the approaches outlined in Passey and Levin (2021) (Fig. 5A). To do this, we assume the
411 triple oxygen isotope fractionation between body water and enamel ($\lambda_{\text{enamel-bw}}$) is similar to that
412 for water and calcite ($\lambda_{\text{calc-water}}$). In recognition that $\lambda_{\text{enamel-bw}}$ may be different than 0.5245, we
413 explored how changing $\lambda_{\text{enamel-bw}}$ affects model output. Figure 5B displays how a decrease in
414 $\lambda_{\text{enamel-bw}}$ to 0.5237 results in a downward shift in the $\Delta'^{17}\text{O}$ results from all four models so they
415 span our observed results.

416 Regardless of the specific $\lambda_{\text{enamel-bw}}$ used, the four modeled scenarios span the range in
417 $\Delta'^{17}\text{O}_{\text{enamel}}$ values observed (Fig. 5). The standard evaporation-sensitive scenario (Model 1)
418 captures minimum $\Delta'^{17}\text{O}$ values that decrease in more arid conditions (low rh), whereas the
419 maximum water dependency model (Model 2) captures the upper range of $\Delta'^{17}\text{O}_{\text{enamel}}$ values
420 where there is little variation with aridity. The outputs from Models 3 and 4 represent variants
421 of these scenarios, with different combinations of WEI and leaf-water consumption, that yield
422 $\Delta'^{17}\text{O}_{\text{enamel}}$ values that plot between those from Models 1 and 2. Changing the WEI adjusts the
423 relative value of $\Delta^{17}\text{O}_{\text{enamel}}$ (low WEI matches low $\Delta'^{17}\text{O}_{\text{enamel}}$), whereas adjusting the proportion of

424 leaf water consumed, changes the sensitivity of $\Delta'{}^{17}\text{O}_{\text{enamel}}$ to rh (consumption of more leaf
 425 water increases sensitivity to rh).

426 The combination of modeled scenarios shows that 1) more water-efficient (low WEI)
 427 animals, such as giraffe and deer, should have lower $\Delta'{}^{17}\text{O}_{\text{enamel}}$ values than less water-efficient
 428 animals (high WEI) like hippos and beavers (Fig. 5) and 2) $\Delta'{}^{17}\text{O}_{\text{enamel}}$ values should decrease with
 429 increasing aridity, especially for animals with low WEI. These outputs capture the trends in the
 430 observed $\Delta'{}^{17}\text{O}_{\text{enamel}}$ data: ES taxa yield lower $\Delta'{}^{17}\text{O}_{\text{enamel}}$ values than EI taxa (Fig. 4B) and $\Delta'{}^{17}\text{O}_{\text{enamel}}$
 431 values decrease with increased aridity (Figs. 3, 5). The model-data comparison here confirms
 432 the strong influences of both diet and physiology and environment on $\Delta'{}^{17}\text{O}_{\text{enamel}}$ values
 433 identified by Passey and Levin (2021) and Hu et al. (*in revision*). $\Delta'{}^{17}\text{O}_{\text{enamel}}$ varies within a guild of
 434 mammals in a single environment, due to differences in behavior, physiology, water-use
 435 strategy, and also across environments.



436

437

438 **Figure 5:** Observed $\Delta'{}^{17}\text{O}_{\text{enamel}}$ values from this study compared to how modeled outputs of
 439 $\Delta'{}^{17}\text{O}_{\text{enamel}}$ values vary with relative humidity (rh), based on a version of the Kohn (1996) model

440 that is modified for triple oxygen isotopes (Passey and Levin, 2021; Hu et al. *in revision*). Each
441 line represents modeled outputs using different diet-physiology scenarios (Models 1-4), where
442 WEI, feces water content, and drinking water amounts vs. leaf water consumption are varied.
443 Modeled body water $\Delta'{}^{17}\text{O}$ values are converted to $\Delta'{}^{17}\text{O}_{\text{enamel}}$ assuming ${}^{18/16}\alpha_{\text{enamel-bw}} = 1.0332$
444 using the approaches outlined in Passey and Levin (2021) and varying the value used for $\lambda_{\text{enamel-}}$
445 $_{\text{bw}}$ (0.5245 vs. 0.5237).

446

447

448 *4.2. Applying $\Delta'{}^{17}\text{O}_{\text{enamel}}$ from large mammalian herbivores to reconstruct past aridity*

449 Considering the generalized $\Delta'{}^{17}\text{O}_{\text{enamel}}$ – aridity relationship among extant animals,
450 across a range of geographic and climate settings, we suggest that $\Delta'{}^{17}\text{O}_{\text{enamel}}$ of fossils can be
451 used to assess past aridity. In the following text we discuss the use of $\Delta'{}^{17}\text{O}_{\text{enamel}}$ values of fossil
452 mammalian herbivores as an indicator of past aridity and the advantages to using $\Delta'{}^{17}\text{O}_{\text{enamel}}$
453 values rather than approaches that rely on $\delta^{18}\text{O}_{\text{enamel}}$ alone.

454

455 *4.2.1. $\Delta'{}^{17}\text{O}_{\text{enamel}}$ as an indicator of aridity*

456 The $\Delta'{}^{17}\text{O}_{\text{enamel}}$ data from modern mammalian herbivores plot in a wedge-shaped pattern
457 with AI that is consistent across geographic regions and among different taxa; the variance in
458 $\Delta'{}^{17}\text{O}_{\text{enamel}}$ values is greatest in more arid environments. Translating this to the fossil record
459 means that variations of $\Delta'{}^{17}\text{O}_{\text{enamel}}$ values from fossil assemblages may be used to infer relative
460 differences in aridity between sites, such that sites with greater variance in $\Delta'{}^{17}\text{O}_{\text{enamel}}$ values
461 represent more arid conditions than sites where $\Delta'{}^{17}\text{O}_{\text{enamel}}$ values are tightly clustered.

462 When using $\Delta^{17}\text{O}_{\text{enamel}}$ values of fossils to compare aridity between sites and through
463 time, sample sets should include taxa from the full range of water-use strategies available in a
464 fossil assemblage. This increases the chances for $\Delta^{17}\text{O}_{\text{enamel}}$ values in the sample set to capture
465 the range in $\Delta^{17}\text{O}_{\text{enamel}}$ values among a population from one place. In our study of extant
466 mammals, we targeted teeth from animals with a range of water-use strategies from each site,
467 but limited our analysis to only two samples for many sites to keep the analytical scope of the
468 project manageable (e.g., hippopotamids/elephantids vs. giraffids) (Supplementary Table 1).
469 Even with limited sampling, we observe greater variation in $\Delta^{17}\text{O}_{\text{enamel}}$ values with increasing
470 aridity. We would likely observe a greater variation in $\Delta^{17}\text{O}_{\text{enamel}}$ values with bigger sample sizes,
471 meaning that the variation in $\Delta^{17}\text{O}_{\text{enamel}}$ values from any place would only provide an indication
472 of minimum aridity for a site.

473 In the most basic sense, $\Delta^{17}\text{O}_{\text{enamel}}$ values of fossil teeth can be used as a way to gage
474 relative differences in aridity between fossil sites. However, the results of $\Delta^{17}\text{O}_{\text{enamel}}$ from fossils
475 can also be considered in terms of the UNESCO climate categories. Pooling our observations
476 from three continents, the expected ranges for $\Delta^{17}\text{O}_{\text{enamel}}$ values from guilds of mammalian
477 herbivores are approximately 50 per meg in humid climates, 120 per meg in semi-arid climates,
478 and 140 per meg in arid climates (Figs. 3B, 3E). We expect adjustments to these values as more
479 individuals, taxa, and environments are sampled and added to this global dataset.

480

481 4.2.2. Advantages of using $\Delta^{17}\text{O}$ as an aridity indicator compared to using $\delta^{18}\text{O}_{\text{enamel}}$ alone

482 The relationship between $\Delta^{17}\text{O}_{\text{enamel}}$ values and aridity is compelling as a paleoaridity
483 indicator because it persists across a wide range of sites, with varying geography and $\delta^{18}\text{O}$

484 values of meteoric water, and among different combinations of mammalian taxa. In contrast,
485 we do not observe similarly clear relationships between $\delta^{18}\text{O}_{\text{enamel}}$ values and aridity because
486 $\delta^{18}\text{O}_{\text{enamel}}$ values are influenced by many other parameters in addition to aridity. As such,
487 $\delta^{18}\text{O}_{\text{enamel}}$ based reconstructions of aridity depend on the identification of taxa that fit into clear
488 ES and EI categories to control for the varying isotopic composition of local waters, but this
489 limits the extent of its application (e.g., Blumenthal et al., 2017).

490

491 *4.2.3. Application guidelines*

492 Below we outline an approach for sampling fossil mammalian herbivore teeth for the
493 purpose of estimating paleoaridity from $\Delta^{17}\text{O}_{\text{enamel}}$ values. We present different scenarios based
494 on sample availability and provide suggestions for how $\Delta^{17}\text{O}_{\text{enamel}}$ data from fossils can be
495 compared with the modern dataset and then placed in a UNESCO climate category.

496 Sample sizes. In this study, we were not able to analyze more than one individual per
497 taxon for many sites, but for the places where we did sample more than one individual per
498 taxon, we find limited variation in $\Delta^{17}\text{O}_{\text{enamel}}$ values amongst individuals (e.g., Turkana hippos: -
499 153 ± 0.7 per meg, $n=2$; Garamba giraffes -203 ± 10 per meg, $n=2$). Given this we conclude that
500 $\Delta^{17}\text{O}_{\text{enamel}}$ data from a single animal provide valuable information, especially if from an ES taxon.
501 Whenever possible, sample sets should include more than one specimen of each taxon to
502 estimate intra-taxon variability of $\Delta^{17}\text{O}_{\text{enamel}}$ values. However, given the fidelity of $\Delta^{17}\text{O}_{\text{enamel}}$
503 values to environment, intra-taxon variability is expected to be relatively small.

504 Limited specimens. Considering that it is not always possible to sample numerous teeth
505 from a site (e.g., poor preservation, restricted sampling permission), we recommend targeting

506 samples that represent a range of water-use strategies to capture the greatest possible
507 $\Delta'^{17}\text{O}_{\text{enamel}}$ variation. If on the other hand you can only sample a few taxa, then water-efficient
508 taxa should be prioritized as their $\Delta'^{17}\text{O}_{\text{enamel}}$ values are likely to represent the minimum
509 $\Delta'^{17}\text{O}_{\text{enamel}}$ values from a place, which could then be compared to $\Delta'^{17}\text{O}_{\text{enamel}}$ values of water-
510 efficient taxa from other fossil sites to assess distinctions in aridity between sites. Our data
511 show that site differences in $\Delta'^{17}\text{O}_{\text{enamel}}$ can help identify environmental distinctions when
512 $\delta^{18}\text{O}_{\text{enamel}}$ cannot. For example, the giraffid $\Delta'^{17}\text{O}_{\text{enamel}}$ values arid sites are the most negative
513 values in the entire dataset and are within 8 per meg of each other, with -278 ± 10 and -283 ± 3
514 per meg, for Kgalagadi and Turkana, respectively (Supplementary Table 1). This similarity is
515 likely due to the arid ($\text{AI} < 0.2$) conditions of both places, despite differences in latitude ($\sim 4.6^\circ\text{N}$
516 vs $\sim 25.7^\circ\text{S}$), annual temperature (28°C vs 20°C), and $\delta^{18}\text{O}$ value for average annual meteoric
517 water ($\sim 1\text{\textperthousand}$ vs $\sim -5\text{\textperthousand}$ VSMOW). In contrast, the $\delta^{18}\text{O}_{\text{enamel}}$ values of these two giraffids are
518 indistinguishable from the $\delta^{18}\text{O}_{\text{enamel}}$ values of giraffids from mesic and humid sites (Fig. 3D).

519 Unknown ES and EI assignment. If there is limited *a priori* knowledge of the behaviors,
520 physiologies, and water-use strategies from fossil herbivores at a site, and it is difficult to target
521 a range of taxa that represent both ES and EI taxa, then a variety of taxa should be sampled to
522 increase the potential of capturing the full range of $\Delta'^{17}\text{O}_{\text{enamel}}$ values at a site. By including taxa
523 with a variety of water-use strategies, a dataset is more likely to capture the range in $\Delta'^{17}\text{O}_{\text{enamel}}$
524 values that represents a site's environment.

525

526 4.3. Other geological applications for $\Delta'^{17}\text{O}_{\text{enamel}}$ of large mammalian herbivores

527 4.3.1. Past $p\text{CO}_2$

528 We are not aware of other studies that propose the use of $\Delta'^{17}\text{O}_{\text{enamel}}$ values as indicators
529 of paleoaridity, but a handful of recent studies have suggested the use of $\Delta'^{17}\text{O}$ values from
530 teeth and eggshells to constrain past atmospheric $p\text{CO}_2$ (Pack et al., 2013; Gehler et al., 2016;
531 Passey et al., 2014; Passey and Levin, 2021). This is an exciting development given the
532 importance of understanding the history of Earth's $p\text{CO}_2$. This approach has been applied to
533 reconstruct $p\text{CO}_2$ across the Paleocene-Eocene Thermal Maximum (PETM); Gehler et al. (2016)
534 use a 60 per meg decrease in $\Delta'^{17}\text{O}_{\text{enamel}}$ values across the PETM to infer a ca. 400 to 1000 ppm
535 increase in atmospheric $p\text{CO}_2$. This approach works because inhaled atmospheric O_2 , which has
536 a $\Delta'^{17}\text{O}$ value considerably lower than any form of water (Fig. 1), contributes between 5% to
537 40% of mammalian body water oxygen. As such, the $\Delta'^{17}\text{O}$ value of atmospheric O_2 is apparent
538 in tooth enamel $\Delta'^{17}\text{O}$ values; it pushes the $\Delta'^{17}\text{O}$ values of body water and enamel more
539 negative than the influences of food and drinking water oxygen alone (Pack et al., 2013). The
540 $\Delta'^{17}\text{O}$ value of atmospheric O_2 is influenced by mass independent fractionation of oxygen
541 isotopes in the stratosphere, where higher concentrations of atmospheric CO_2 leads to
542 decreased $\Delta'^{17}\text{O}$ values of atmospheric O_2 (Luz et al., 1999; Bao et al., 2008), and in turn, lower
543 $\Delta'^{17}\text{O}_{\text{enamel}}$ values (Pack et al., 2013).

544 Currently, $\Delta'^{17}\text{O}_{\text{enamel}}$ -based estimates of $p\text{CO}_2$ are calculated from animals with small
545 body mass and high respiration rates (Gehler et al., 2016). These estimates do not consider how
546 $\Delta'^{17}\text{O}_{\text{enamel}}$ values vary among taxa (aside from differences in body mass) or in different
547 environments. But such variation is important; a 60 per meg distinction in $\Delta'^{17}\text{O}_{\text{enamel}}$ values that
548 is used to infer changes in $p\text{CO}_2$ can also be observed within an arid location among different
549 animals (e.g., Turkana) or between environments (e.g., 60 per meg represents the difference

550 between a subhumid and arid environment; Fig. 3). Given the similar magnitude of change in
551 $\Delta'^{17}\text{O}_{\text{enamel}}$ values that occurs with a change in environment, animal taxon, or $p\text{CO}_2$ it will be
552 essential to characterize the influence of environment on $\Delta'^{17}\text{O}_{\text{enamel}}$ values of mammalian
553 herbivores before using them to infer $p\text{CO}_2$. To do this, we suggest sampling teeth from a range
554 of taxa and from multiple fossil sites within a single time interval. Sites from a single time period
555 across the globe should have similar atmospheric $p\text{CO}_2$. If $p\text{CO}_2$ is significantly different from
556 today, then there will be a wholesale shift in $\Delta'^{17}\text{O}_{\text{enamel}}$ values away from the modern
557 distribution of $\Delta'^{17}\text{O}_{\text{enamel}}$ values across multiple fossil sites, environments, and populations of
558 taxa. We recognize that assessing past $p\text{CO}_2$ using $\Delta'^{17}\text{O}_{\text{enamel}}$ will require further study, but any
559 use of $\Delta'^{17}\text{O}_{\text{enamel}}$ as a proxy for CO_2 needs to consider environmental and taxonomic variation in
560 $\Delta'^{17}\text{O}_{\text{enamel}}$ values.

561

562 4.3.2. *Diagenesis*

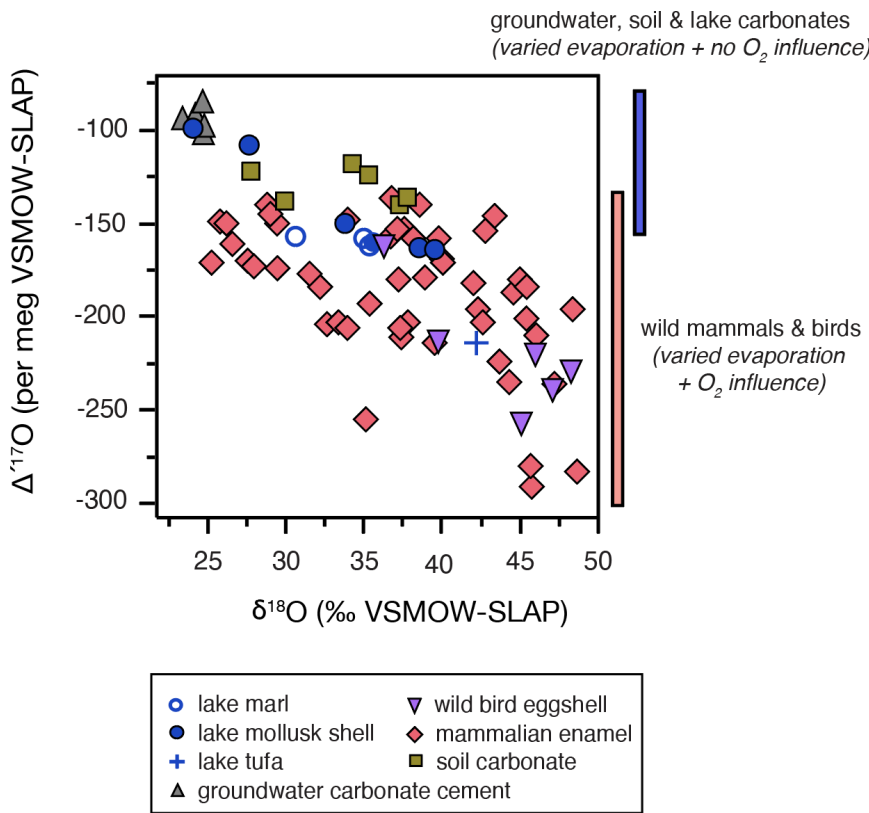
563 Assessing and accounting for the role of diagenesis on $\delta^{18}\text{O}$ values of biocarbonate (i.e.,
564 tooth, bone, eggshell) has been a longstanding challenge in their use for paleoclimate
565 reconstructions (e.g., Iacumin et al., 1996; Schoeninger et al., 2003). Any post-depositional
566 reprecipitation of carbonate reflects the temperatures and isotopic composition of waters of
567 this secondary event, not the biomineralization in an animal. The influence of reprecipitated
568 carbonate on $\delta^{18}\text{O}_{\text{enamel}}$ values can be evaluated by comparing $\delta^{18}\text{O}_{\text{enamel}}$ values among different
569 taxa, the $\delta^{18}\text{O}$ of phosphate in the same tooth enamel, or to the $\delta^{18}\text{O}$ of sedimentary
570 carbonates. The elemental composition of bioapatite using x-ray diffraction and infrared
571 spectroscopy can also be analyzed (e.g., Person et al., 1995; Iacumin et al., 1996).

572 The triple oxygen isotope composition of carbonates and bioapatites provides another
573 way to evaluate the effects of diagenesis (Gehler et al., 2011). Animal tissue $\Delta^{17}\text{O}$ values are
574 more negative and more variable than the $\Delta^{17}\text{O}$ values of carbonates derived from meteoric
575 waters due to the influence of low- $\Delta^{17}\text{O}$ inhaled atmospheric O₂ and the strong roles of
576 environment and animal water-use that results in varying $\Delta^{17}\text{O}$ values (Fig. 6).

577 The clear distinction between $\Delta^{17}\text{O}$ values of biological carbonates and meteoric
578 carbonates means that $\Delta^{17}\text{O}$ measurements can be used to evaluate diagenesis of the original
579 oxygen isotopic composition of bicarbonate without relying on additional analyses and
580 materials. Gehler et al. (2011) suggests the $\Delta^{17}\text{O}$ values of tissue from small mammals (< 1 kg)
581 can help evaluate diagenesis. This concept is also relevant for larger mammals (> 6 kg) and
582 birds, as $\Delta^{17}\text{O}$ values of tooth enamel and eggshells are more negative and more variable than
583 those of meteoric-derived carbonates (Fig. 6). However, there are some exceptions; carbonates
584 formed from waters that are extensively evaporated, such as closed basin, saline Mono Lake,
585 can have $\Delta^{17}\text{O}$ values as low as -214 per meg (see Passey and Ji, 2019) and fall squarely in the
586 range of $\Delta^{17}\text{O}$ values of bird and mammal bicarbonate.

587 To use $\Delta^{17}\text{O}$ analyses to determine diagenesis of fossil enamel, a sample set should
588 include both fossils from taxa with a range of water-use strategies and carbonates that are
589 available from the sediments associated with the fossils (e.g., soil carbonate, lacustrine
590 carbonate, cements). If the $\Delta^{17}\text{O}_{\text{enamel}}$ values are unaltered, then they will be more negative and
591 varied than that of the associated carbonates. If the $\Delta^{17}\text{O}$ values of carbonates and enamel are
592 similar, then the distribution of $\Delta^{17}\text{O}_{\text{enamel}}$ values will be compressed and the original oxygen

593 isotopic composition of the fossil teeth has been altered. This concept can be extended to other
594 fossil biocarbonates like bones and eggshells.



595

596

597 **Figure 6:** The $\Delta^{17}\text{O}$ and $\delta^{18}\text{O}$ values of large mammalian tooth enamel, bird eggshells, mollusks,
598 and groundwater cement, lake, and soil carbonates. Data are from Passey et al. (2014), Passey
599 and Ji (2019), Hu et al. (*in revision*), and this study.

600

601

602 **5. Conclusions**

603 The $\Delta^{17}\text{O}_{\text{enamel}}$ values of extant, large mammalian herbivores sampled from three
604 continents and seven mammalian families vary by 146 per meg (-283 to -137 per meg). The

605 relationship between $\Delta'^{17}\text{O}_{\text{enamel}}$ values and aridity form a wedge-shaped pattern, with greater
606 variation in $\Delta'^{17}\text{O}_{\text{enamel}}$ values in arid environments. This relationship is independent of latitude
607 and $\delta^{18}\text{O}$ value of local meteoric waters. However, the relationship between $\Delta'^{17}\text{O}_{\text{enamel}}$ values
608 does depend on animal water-use strategy; generally, $\Delta'^{17}\text{O}_{\text{enamel}}$ values from water-dependent
609 animals vary little with aridity, whereas water-efficient animals yield lower $\Delta'^{17}\text{O}_{\text{enamel}}$ values that
610 decrease with aridity.

611 Our dataset provides a framework for using $\Delta'^{17}\text{O}_{\text{enamel}}$ values to evaluate aridity of past
612 environments. The $\Delta'^{17}\text{O}_{\text{enamel}}$ values from multiple taxa in a fossil assemblage can be used to
613 estimate the paleoaridity of a fossil site and roughly place it into one of the UNESCO climate
614 categories. The use of $\Delta'^{17}\text{O}_{\text{enamel}}$ values broadens the utility of the oxygen isotope composition
615 of terrestrial materials for paleoenvironmental reconstructions, because their distribution is so
616 tied to aridity, unlike $\delta^{18}\text{O}$ values of enamel (and other materials) which are influenced by a
617 combination of multiple factors (e.g., aridity, temperature, $\delta^{18}\text{O}$ values of meteoric water).

618 In addition to their utility for paleoenvironmental reconstructions, $\Delta'^{17}\text{O}$ values of fossil
619 teeth can be used to estimate past $p\text{CO}_2$ and evaluate diagenetic effects on the oxygen isotope
620 composition of samples. Our expanded dataset from extant herbivores shows the importance
621 of sampling teeth from a range of taxa for both of these approaches to work effectively. Studies
622 that use $\Delta'^{17}\text{O}_{\text{enamel}}$ values as a $p\text{CO}_2$ indicator must first account for the range of $\Delta'^{17}\text{O}_{\text{enamel}}$
623 variation due to the environment and animal water-use strategy. Likewise, any study using
624 $\Delta'^{17}\text{O}_{\text{enamel}}$ values to identify diagenesis should include samples from taxa with different water-
625 use strategies because they should yield $\Delta'^{17}\text{O}_{\text{enamel}}$ values that are relatively wide-ranging if
626 unaltered and relatively invariant if altered. These results show the expanded potential for the

627 utility of triple oxygen isotope distributions in biocarbonates. The next steps for this work
628 include expanding the sample from extant animals to include more individuals from a broader
629 range of geographic settings and then applying this framework to constrain aridity, $p\text{CO}_2$, and
630 diagenesis in Earth's past.

631

632

633 **Acknowledgements**

634 We thank David Patterson, Scott Blumenthal, and staff from the Edness Kimball Wilkins State
635 National Park, WY for providing samples for analysis. We also thank Scott Blumenthal for
636 sharing his Matlab code for extracting water isotope data from WorldClim 1.4 and for
637 assistance in extracting climate information for each site. We thank the Department of Earth
638 and Planetary Sciences Department at Johns Hopkins University where samples were prepared
639 and analyzed. A Johns Hopkins Early Career Catalyst Grant awarded to Naomi Levin funded this
640 work.

641 **Figure list**

642 Figure 1: $\Delta'^{17}\text{O}$ and $\delta^{18}\text{O}$ values of waters and reconstructed waters from carbonates.

643

644 Figure 2: Schematic outlining the variation of $\delta^{18}\text{O}_{\text{enamel}}$ and $\Delta'^{17}\text{O}_{\text{enamel}}$ values with aridity for

645 different mammalian herbivore taxa.

646

647 Figure 3: Variation in $\delta^{18}\text{O}_{\text{enamel}}$ and $\Delta'^{17}\text{O}_{\text{enamel}}$ values by latitude, location, taxon, and climate.

648

649 Figure 4: Box plots of (A) $\delta^{18}\text{O}_{\text{enamel}}$ and (B) $\Delta'^{17}\text{O}_{\text{enamel}}$ of taxa grouped by evaporation sensitivity.

650

651 Figure 5: The $\Delta'^{17}\text{O}$ and $\delta^{18}\text{O}$ values of large mammalian tooth enamel, bird eggshells, and lake

652 and soil carbonates.

653

654 Figure S1: Distribution of (a) $\delta^{18}\text{O}_{\text{enamel}}$ and (b) $\Delta'^{17}\text{O}_{\text{enamel}}$ data. From left to right: Histogram of

655 data with a normal continuous fit. Quantile box plot with horizontal lines as median and

656 quantile groups, points as outliers, and brackets as the region of densest data. Normal quantile

657 plot with line of fit, the empirical cumulative probability and normal quantile scales, and

658 Lilliefors confidence bounds (dotted line).

659

660 **Table List**

661 Table 1. Geographic, climatic and environmental information for sample locations.

662

663 Table 2: Animal behavior summary for reported taxa.

664

665 Table S1. Compilation of oxygen isotope data for tooth enamel specimens and calculated body

666 waters.

667

668 Table S2. References of original papers for tooth enamel samples.

669

670 Table S3. Summaries of standards from analytical sessions.

671

672 Table S4. Raw data and standards from session runs.

673

674 Table S5. Statistical tests of significance between families in different regions.

675

676 Table S6. Conditions of body water model scenarios for different diet physiologies.

677

678 Table S7. Modeled body water and enamel oxygen isotopes based on input and output

679 parameters in relation to diet, physiology, and environment.

680

681 Table S8. Modeled body water and enamel oxygen isotopes with relative humidity and Aridity

682 Index.

683

684 **Table 1.** Geographic, climatic and environmental information for sample locations.

685

Country	Location	Latitude	Longitude	CRU output mean rh (%)	OIPC 3.1 $\delta^{18}\text{O}$ MAP (% SMOW)	RCWIP $\delta^{18}\text{O}$ MAP (% SMOW)	MAP (mm/yr)	MAT (°C)	PET (mm/yr)	WD (mm/yr)	Aridity Index	Aridity Index UNESCO category
Africa												
Kenya	Turkana	4.3641	35.663	52.9	1.1	0.2	347	28	1897	1550	0.18	arid
Kenya	Meru National Park	0.0806	38.1979	63.2	1.7	-0.5	512	24.5	2064	1552	0.24	semi-arid
Kenya	Shimba Hills National Park	-4.2572	39.3878	70.9	-3.5	-1.4	1137	23.9	1493	356	0.75	semi-arid
Kenya	Laikipia/Mpala National Park	0.348	36.9924	63.9	-0.8	-4.8	713	18.2	1782	1069	0.39	semi-arid
Kenya	Tsavo National Park	-2.3661	38.4098	63.3	0.8	-1.3	670	25	1836	1166	0.37	semi-arid
Kenya	Aberdares National Park	-0.4359	36.717	70.2	-3.6	-9.0	1780	10.1	1196	-584	1.52	humid
Ethiopia	Awash National Park	9.0833	40	62.6	2.2	-1.0	525	25.9	2091	1566	0.25	semi-arid
Uganda	Kidepo National Park	3.8604	33.8549	57.9	-1.1	-1.7	614	22.9	1720	1106	0.34	semi-arid
DR Congo	Garamba National Park	4.1665	29.5003	67.1	0.2	-1.5	1548	24.4	1813	265	0.86	humid
DR Congo	Ituri Forest National Park	1.4043	28.5769	71.6	-0.2	-2.1	1739	24.4	1771	32	0.98	humid
South Africa	Kgalagadi National Park	-25.7488	20.4436	43.8	-4.7	-3.7	230	20	1878	1648	0.12	arid
South Africa	Addo National Park	-33.5023	25.7721	64.2	-3.7	-3.2	424	17.9	1398s	974	0.32	semi-arid
Europe												
Finland	Noormarkku	61.5908	21.8671	81.6	-12.0	-11.5	608	4	548	-60	1.11	humid
Finland/Sweden	Karessuando	68.438	22.4511	86.5	-14.9	-14.2	448	-2.2	393	-55	1.14	humid
Finland	Rovaniemi	66.5181	25.669	80.0	-13.1	-13.5	513	0.4	458	-55	1.13	humid
Finland	Pernaja	60.4386	26.0528	81.1	-11.8	-11.8	618	4.7	547	-71	1.13	humid
Karelia, Russia	Aunus Nurmoila	61.07513	32.924	81.8	-12.0	-12.3	672	2.9	541	-131	1.24	humid
North America												
United States	Badlands National Park, SD	43.8554	-102.34	60.5	-9.9	-11.5	415	8.6	1109	694	0.37	semi-arid
United States	Theodore Roosevelt National Park, ND	46.979	-103.539	63.9	-11.4	-13.0	383	6.3	982	599	0.40	semi-arid
United States	Wichita Mountains Federal Wildlife Refuge, OK	34.7223	-98.7345	63.7	-5.8	-6.7	735	15.4	1358	623	0.54	subhumid
United States	Antelope Island, UT	40.9581	-112.215	54.3	-14.1	-10.1	462	10.1	1026	564	0.57	subhumid
United States	Parowan, UT	37.8352	-112.829	48.1	-12.7	-11.7	320	8.9	1229	909	0.26	semi-arid
United States	Arctic National Wildlife Refuge, AK	68.6496	-142.898	67.9	-26.0	-24.2	154	-13.9	263	109	0.58	subhumid
United States	Middle Fork, Selman River, ID	44.9305	-114.965	59.9	-16.6	-15.1	581	-0.1	789	208	0.74	subhumid
United States	Piedmont National Wildlife Refuge, GA	33.0864	-83.7275	70.2	-5.5	-5.5	1213	17.3	1415	202	0.86	humid
United States	Berkley Springs, WV	39.6249	-78.2387	69.6	-8.2	-8.0	949	10.7	1093	144	0.87	humid
United States	Baltimore, MD	39.3068	-76.6316	66.6	-6.7	-6.5	1110	12.9	1142	32	0.96	humid
United States	Westchester County, NY	41.122	-73.7949	67.7	-7.6	-8.3	1227	10.6	980	-247	1.26	humid
United States	Dairymens Country Club, WI	46.1453	-89.6576	72.6	-10.8	-11.9	834	3.8	819	-15	1.02	humid
United States	Yellowstone National Park, WY	44.428	-110.588	55.7	-16.8	-17.2	646	-1	760	114	0.82	humid
United States	Edness Kimball Wilkins State National Park, WY	42.8536	-106.182	55.3	-13.0	-12.9	311	7.9	1105	794	0.28	semi-arid

686
687

688 **Table 2.** Animal behavior summary for reported taxa

Common name	Family	Genus and species	Diet	General water use strategy	ES or EI status ^a
Red/Cape hartebeest	Bovidae	<i>Alcelaphus buselaphus caama</i>	Grazer	^{e, i} Not very water dependent	-
Bison	Bovidae	<i>Bison bison bison</i>	Grazer	^h Water dependent	EI
Blue wildebeest	Bovidae	<i>Connochaetes taurinus taurinus</i>	Grazer	ⁱ Not very water dependent	-
Oryx	Bovidae	<i>Oryx gazella beisa</i>	Grazer	^{b, e, i} Not water dependent	ES
African buffalo	Bovidae	<i>Synacerus caffer</i>	Grazer	^{e, i} Water dependent	-
Beaver	Castoridae	<i>Castor fiber</i>	Semi-aquatic	^d Water dependent	EI
Moose	Cervidae	<i>Alces alces</i>	Mixed feeder/Semi-aquatic	^d Water dependent	EI
White-tailed deer	Cervidae	<i>Odocoileus virginianus virginianus</i>	Mixed feeder	^c Not water dependent	ES
Reindeer and Caribou	Cervidae	<i>Rangifer tarandus</i>	Browser/Mixed feeder	^d Not very water dependent	-
Elephant	Elephantidae	<i>Loxodonta africana africana</i>	Browser	ⁱ Water dependent	EI
Giraffe	Giraffidae	<i>Giraffa camelopardalis</i>	Browser	^{g, i} Not water dependent	ES
Okapi	Giraffidae	<i>Okapia johnstoni</i>	Browser	^{f, g, i} Not water dependent	ES
Hippo	Hippopotamidae	<i>Hippopotamus amphibius amphibius</i>	Semi-aquatic	^{g, i} Water dependent	EI
Black rhino	Rhinocerotidae	<i>Diceros bicornis</i>	Browser/Grazer	ⁱ Water dependent	EI

^a Data are classified as ES or EI based on the relationship between $\delta^{18}\text{O}$ values and aridity and relative humidity based on previously published work. For taxa that have not been classified as ES and EI, we evaluated their diet, water use, and WEI when available to suggest ES or EI classification.

References ^bKohn et al., 1996; ^cLuz et al., 1990; ^dNowak, 1991; ^{e,f}Cerling et al., 2003; 2004; ^gLevin et al., 2006; ^hHoppe et al., 2006; ⁱBlumenthal et al. 2017)

689

690

691 **References**

- 692 Alexandre, A., Landais, A., Vallet-Coulomb, C., Piel, C., Devidal, S., Pauchet, S., Sonzogni, C.,
693 Couapel, M., Pasturel, M., Cornuault, P., Xin, J., Mazur, J.-C., Prié, F., Bentaleb, I., Webb, E.,
694 Chalié, F., Roy, J., 2018. The triple oxygen isotope composition of phytoliths as a proxy of
695 continental atmospheric humidity: insights from climate chamber and climate transect
696 calibrations. *Biogeosciences.* 15, 3223-3241.
- 697
- 698 Bao, H., Lyons, J.R., Zhou, C., 2008. Triple oxygen isotope evidence for elevated CO₂ levels after
699 a Neoproterozoic glaciation. *Nature.* 453, 504-506.
- 700
- 701 Barkan, E., Luz, B., 2005. High precision measurements of ¹⁷O/¹⁶O and ¹⁸O/¹⁶O ratios in H₂O.
702 *Rapid Communications of Mass Spectrometry.* 19, 3737-3742.
- 703
- 704 Barkan, E., Luz, B., 2007. Diffusivity fractionations of H₂¹⁶O/H₂¹⁷O and H₂¹⁶O/H₂¹⁸O in air and their
705 implications for isotope hydrology. *Rapid Communications of Mass Spectrometry.* 21,
706 2999-3005.
- 707
- 708 E. Barkan, E., Luz, B., 2011. The relationships among the three stable isotopes of oxygen in air,
709 seawater and marine photosynthesis. *Rapid Commun. Mass Spectrom.* 25, 2367-2369.
- 710
- 711 Blumenthal, S.A., Levin, N.E., Cerling, T.E., Brown, F.H., Brugal, J.-P., Chritz, K.L., Harris, J.M.,
712 Jehle, G.E., 2017. Aridity and early hominin environments. *Proceedings of the National*

- 713 Academy of Sciences. 114, 7331-7336.
- 714 Bowen, G.J., Revenaugh, J., 2003. Interpolating the isotopic composition of modern meteoric
715 precipitation. Water Resour. Res. 39, 1299.
- 716 Bryant J. D. and Froelich P. N. (1995) A model of oxygen isotope fractionation in body water of
717 large mammals. Geochim Cosmochim Acta 59, 4523–4537.
- 718
- 719 Dansgaard, W., 1964. Stable Isotopes in Precipitation. Tellus. 16, 436-468.
- 720
- 721 Fricke, H.C., O'Neil, J.R., Lynnerup, N., 1995. Oxygen isotope composition of human tooth
722 enamel from Medieval Greenland: linking climate and society. Geology. 23, 869-872.
- 723
- 724 Gehler, A., Gingerich, P.D., Pack, A., 2016. Temperature and atmospheric CO₂ concentration
725 estimates through the PETM using triple oxygen isotope analysis of mammalian bioapatite.
726 Proceedings of the National Academy of Sciences. 113, 7739-7744.
- 727
- 728 Gehler, A., Tütken, T., Pack, A., 2011. Triple oxygen isotope analysis of bioapatite as tracer for
729 diagenetic alteration of bones and teeth. Paleogeography, Paleoceanography, Paleoecology. 310,
730 84-91.
- 731
- 732 Herwartz, D., Surma, J., Voigt, C., Assonov, S., Staubwasser, M., 2017. Triple oxygen isotope
733 systematics of structurally bonded water in gypsum. Geochimica Cosmochimica Acta 209. 254-

- 734 266.
- 735
- 736 Hijmans, R.J., Cameron, S.E., Parra, J.L., Jones, P.G., Jarvis, A., 2005. Very high resolution
737 interpolated climate surfaces for global land areas. *Int. J. Climatol.* 25, 1965-1978.
- 738
- 739 Hu, H., Passey, B.H., Lehmann, S.B., Levin, N.E., Johnson, B.J., (*in revision*). Modeling and
740 interpreting triple oxygen isotope variations in vertebrates, with implications for paleoclimate
741 and paleoecology. *Chemical Geology*.
- 742
- 743 Iacumin, P., Bocherens, H., Mariotti, A., Longinelli, A., 1996. Oxygen isotope analyses of co-
744 existing carbonate and phosphate inn biogenic apatite: a way to monitor diagenetic alteration
745 of bone phosphate? *Earth and Planetary Science Letters*. 142, 1-6.
- 746
- 747 Kohn, M.J., 1996. Predicting animal $\delta^{18}\text{O}$: accounting for diet and physiological adaptation.
748 *Geochimica et Cosmochimica Acta*. 60, 4811-4829.
- 749
- 750 Landais, A., Barkan, E., Yakir, D., Luz, B., 2006. The triple isotopic composition of oxygen in leaf
751 water. *Geochimica et Cosmochimica Acta*. 70, 4105-4115.
- 752
- 753 Landais, A., Risi, C., Bony, S., Vimeux, F., Descroix, L., Falourd, S., Bouygues, A., 2010. Combined
754 measurement of ^{17}O -excess and d-excess in African monsoon precipitation: Implication for
755 evaluating convective parameterizations. *Earth and Planetary Science Letters*. 298, 104-112.

756

757 Lécuyer, C., Balter, V., Martineau, F., Fourel, F., Bernard, A., Amiot, R., Gardien, V., Otero, O.,
758 Legendre, S., Panczer, G., Simon, L., Martini, R., 2010. Oxygen isotope fractionation between
759 apatite-bound carbonate and water determined from controlled experiments with synthetic
760 apatites precipitated at 10-37°C. *Geochimica et Cosmochimica Acta.* 74, 2072-2081.

761

762 Levin, N.E., Cerling, T.E., Passey, B.H., Harris, J.M., Ehleringer, J. R., 2006. A stable isotope aridity
763 index for terrestrial environments. *Proceedings of the National Academy of Sciences.* 103,
764 11201-11205.

765

766 Li, S., Levin, N.E., Soderberg, K., Dennis, K.J., Taylor, K.K., 2017. Triple oxygen isotope
767 composition of leaf waters in Mpala, central Kenya. *Earth and Planetary Science Letters.* 468,
768 38-50.

769

770 Luz, B., Cormie, A.B., Schwarcz, H.P., 1990. Oxygen isotope variations in phosphate of deer
771 bones. *Geochimica et Cosmochimica Acta.* 54, 1723-1728.

772

773 Luz, B., Barkan, E., Bender, M.L., Thiemens, M.H., Boering, K.A., 1999. Triple-isotope
774 composition of atmospheric oxygen as a tracer of biosphere productivity. *Nature.* 400, 547-550.

775

776 Luz, B., Barkan, E., 2005. The isotopic ratios $^{17}\text{O}/^{16}\text{O}$ and $^{18}\text{O}/^{16}\text{O}$ in molecular oxygen and their
777 significance in biogeochemistry. *Geochimica et Cosmochimica Acta.* 69, 1099-1110.

778

779 Luz, B., Barkan, E., 2010. Variations of $^{17}\text{O}/^{16}\text{O}$ and $^{18}\text{O}/^{16}\text{O}$ in meteoric waters. *Geochimica et Cosmochimica Acta.* 74, 6276-6286.

781

782 Matsuhisa, Y., Goldsmith, J.R., Clayton, R.N., 1978. Mechanisms of hydrothermal crystallization
783 of quartz at 250°C and 15kbar. *Geochimica et Cosmochimica Acta.* 42, 173-182.

784

785 Miller, M.F., 2002. Isotopic fractionation and the quantification of ^{17}O anomalies in the oxygen
786 three-isotope system: an appraisal and geochemical significance. *Geochimica et Cosmochimica
787 Acta.* 66, 1881-1889.

788

789 Nagy, K.A., Peterson, 1988, Scaling of water flux rate in animals. University of California
790 Publications in Zoology, 120, 1-172.

791

792 Nowak, R., 1999, Walker's Mammals of the World. Sixth Edition. Baltimore. The Johns Hopkins
793 University Press.

794

795 Pack, A., 2021. Isotopic traces of atmospheric O₂ in rocks, minerals, and melts. *Reviews in
796 Mineralogy and Geochemistry.* 86, 217-240.

797

798 Pack, A., Gehler, A., Süssenberger, A., 2013. Exploring the usability of isotopically anomalous
799 oxygen in bones and teeth as paleo-CO₂-barometer. *Geochimica et Cosmochimica Acta.* 102,

- 800 306-317.
- 801
- 802 Passey BH, Levin NE. 2021. Triple oxygen isotopes in meteoric waters, carbonates, and
- 803 biological apatites: implications for continental paleoclimate reconstruction. *Reviews in*
- 804 *Mineralogy & Geochemistry*. 86, 429-462.
- 805
- 806 Passey, B.H., Hu, H., Ji, H., Montanari, S., Li, S., Henkes, G.A., Levin, N.E., 2014. Triple oxygen
- 807 isotopes in biogenic and sedimentary carbonates. *Geochimica et Cosmochimica Acta*. 141, 1-25.
- 808
- 809 Passey, B.H., Ji, H., 2019. Triple oxygen isotope signatures of evaporation in lake waters and
- 810 carbonates: A case study from the Western United States. *Earth and Planetary Science Letters*.
- 811 518, 1-12.
- 812
- 813 Person, A., Bocherens, H., Saliège, J.F., Paris, F., Zeitoun, V., Gérard, M., Early Diagenetic
- 814 Evolution of Bone Phosphate: An X-ray Diffractometry Analysis. *Journal of Archaeological*
- 815 *Science*. 22, 211-221.
- 816
- 817 Rowley, D.B., Currie, B.S., 2006. Palaeo-altimetry of the late Eocene to Miocene Lunpola basin,
- 818 central Tibet. *Nature*. 439, 677-681.
- 819
- 820 Rozanski, K., Aragua´s-Aragua´s, L., Gonfiantini, R., 1993. Isotopic patterns in modern global
- 821 precipitation. In: Swart, P.K., Lohmann, K.C., McKenzie, J., Savin, S. (Eds.), *Climate Change in*

- 822 Continental Isotopic Records. American Geophysical Union Geophysical Monograph. American
823 Geophysical Union. Washington, DC. 78, 1-36.
- 824
- 825 Schoenemann, S.W., Schauer, A.J., Steig, E.J., 2013. Measurement of SLAP2 and GISP $\delta^{17}\text{O}$ and
826 proposed VSMOW-SLAP normalization for $\delta^{17}\text{O}$ and $\delta^{18}\text{O}$. Rapid Communications in Mass
827 Spectrometry. 27, 582-590.
- 828
- 829 Schoeninger, M.J., Hallin, K., Reeser, H., Valley, J.W., Fournnelle, J., 2003. Isotopic alteration of
830 mammalian tooth enamel. International Journal of Osteoarchaeology. 13, 11-19.
- 831
- 832 Sharp, Z.D., Wostbrock, J.A.G., 2021. Standardization for the triple oxygen isotope system:
833 Waters, silicates, carbonates, air, and sulfates. Reviews in Mineralogy & Geochemistry. 86, 179-
834 196.
- 835
- 836 Surma, J., Assonov, S., Bolourchi, M.J., Staubwasser, M., 2015. Triple oxygen isotope signatures
837 in evaporated water bodies from the Sistan Oasis, Iran. Geophysical Research Letters. 42,
838 8456-8462.
- 839
- 840 Surma, J., Assonov, S., Herwartz, D., Voigt, C., Staubwasser, M., 2018. The evolution of ^{17}O -
841 excess in surface water of the arid environment during recharge and evaporation. Scientific
842 Reports. 8, 4972.
- 843

844 Trabucco, A., Zomer, R.J., 2009. Global Aridity Index (Global-aridity) and Global Potential Evapo-
845 transpiration (Global-PET) Geospatial Database. CGIAR Consortium for Spatial Information.
846 Published online, available from: the CGIAR-CSI GeoPortal. <http://www.cgiar.org/>.

847

848 Uechi, Y., Uemura, R., 2019. Dominant influence of the humidity in the moisture source region
849 on the ^{17}O -excess in precipitation on a subtropical island. Earth and Planetary Science Letters.
850 513, 20-28.

851

852 UNESCO, 1979. Map of the world distributions of arid regions, explanatory note, MAB Technical
853 Notes, Paris.

854

855 Whiteman, J.P., Sharp, Z.D., Gerson, A.R., Newsome, S.D., 2019. Relating $\Delta^{17}\text{O}$ values of animal
856 body water to exogenous water inputs and metabolism. BioScience. 69, 658-688.

857

858 Wostbrock, J.A.G., Cano, E.J., Sharp, Z.D., 2020, An internally consistent triple oxygen isotope
859 calibration of standards for silicates, carbonates and air relative to VSMOW2 and SLAP2.
860 Chemical Geology 533, 119432.

861

862 Young, E.D., Galy, A., Nagahara, H., 2002. Kinetic and equilibrium mass-dependent isotope
863 fractionation laws in nature and their geochemical and cosmochemical significance. Geochimica
864 et Cosmochimica Acta. 66, 1095-1104.

865

866 Zachos, J., Pagani, M., Sloan, L., Thomas, E., Billups, K., 2001. Trends, rhythms, and
867 aberrations in global climate 65 Ma to present. *Science*. 292, 686-693.